FePt nanoparticles formed in Al_2O_3 by ion beam synthesis: Annealing environment effects

C. W. White[a] and S. P. Withrow
Oak Ridge National Laboratory, Oak Ridge, Tennessee 37831

J. M. Williams
BronteK Delta Corporation, Radford, Virginia 24141

J. D. Budai
Oak Ridge National Laboratory, Oak Ridge, Tennessee 37831

A. Meldrum
The University of Alberta, Edmonton, Canada T6G 2M7

K. D. Sorge
The University of Tennessee, Knoxville, Tennessee 37996

J. R. Thompson
Oak Ridge National Laboratory, Oak Ridge, Tennessee 37831 and The University of Tennessee, Knoxville, Tennessee 37996

L. A. Boatner
Oak Ridge National Laboratory, Oak Ridge, Tennessee 37831

(Received 13 November 2003; accepted 16 March 2004)

The properties of FePt nanoparticles formed by the implantation of Fe+Pt into *c*-axis-oriented Al_2O_3 single crystals followed by thermal annealing are shown to be strongly dependent on the annealing environment. Annealing in a reducing environment (flowing Ar+4% H_2, or ultrahigh vacuum) gives rise to ferromagnetic FePt nanoparticles with the $L1_0$ structure and very high magnetic coercivity (greater than 20 kOe). FePt alloy formation does not occur during annealing in an oxidizing environment. Instead, the implanted Pt precipitates out forming oriented Pt nanoparticles and the implanted Fe redistributes with ~40% segregating to the surface where it forms epitaxial α-Fe_2O_3 precipitates at the surface; the remainder of the implanted Fe remains in the bulk, most likely in solid solution in the matrix. Results obtained by sequential annealing of Fe+Pt implanted samples in reducing (oxidizing) environments followed by annealing in an oxidizing (reducing) environment suggest that equilibrium, rather than kinetic, effects are responsible for the observed microstructures. © *2004 American Institute of Physics.*
[DOI: 10.1063/1.1737806]

I. INTRODUCTION

FePt ordered alloy nanoparticles with the $L1_0$ structure have attracted a high level of interest recently due to their hard ferromagnetic properties.[1] As an ordered alloy, this material has a very high uniaxial magnetocrystalline anisotropy [$K_u \sim 7\times10^6$ J/m^3] and a relatively high magnetization, thus making FePt ordered alloys excellent candidates for ultrahigh density magnetic data storage applications.[2] Nanoparticles of ordered FePt have been synthesized chemically as a superlattice of monodispersed spherical particles,[1] and films of $Fe_{1-x}Pt_x$ (with $x\sim50\%$) with high magnetic anisotropy have been prepared by a number of techniques including molecular beam epitaxy (MBE),[3] cosputtering,[4] sputtering of multilayers,[5] and ion irradiation of deposited multilayers.[6]

Recently, we have used the sequential implantation of Fe and Pt ions, followed by thermal annealing in a reducing environment, to form crystallographically oriented, ordered alloy nanoparticles of $Fe_{1-x}Pt_x$ in single-crystal Al_2O_3 matrices.[7,8] Both the orientation and the microstructures of the FePt nanoparticles depend on the implantation conditions. By varying the relative dose of Fe and Pt, the Pt concentration in the alloy can be altered over a wide range. We have found that the ordered $L1_0$ structure of FePt is formed over a range of concentrations extending from ~35% to 55% Pt. In this range, the $Fe_{1-x}Pt_x$ nanoparticles are ferromagnetic, and the magnetic coercivity is a strong function of the Pt concentration, reaching a coercivity in excess of 20 kOe (measured at $T=5$ K) for an $Fe_{55}Pt_{45}$ alloy.

In the present work, we have investigated the effect of the annealing environment on FePt alloy formation in Al_2O_3. Our results demonstrate that the phase formed, the microstructure, and the associated magnetic properties of the nanoparticles are strongly dependent on the annealing environment for materials formed by implanting Fe+Pt into *c*-axis oriented Al_2O_3 crystals.

[a]Electronic mail: whitecw@solid.ssd.ornl.gov

II. EXPERIMENTAL PROCEDURE

Single crystal substrates of *c*-axis-oriented Al_2O_3 were implanted with Fe (350 keV) followed by Pt (910 keV) to give overlapping profiles of Fe and Pt with a projected range of ~175 nm for each element. Doses of $1\times10^{17}/cm^2$ for Fe and $8.2\times10^{16}/cm^2$ for Pt were used in order to produce an alloy with a nominal Pt atomic fraction of 45% [=Pt dose/(Fe dose+Pt dose)], assuming complete alloying of the implanted Fe and Pt. Our previous work[8] established that the maximum magnetic coercivity occurred for a Pt atomic fraction of 45%. The ion implantation was carried out at elevated temperatures (550 °C for Fe and 500 °C for Pt) in order to prevent the near surface of the Al_2O_3 substrate from being rendered amorphous by implantation-induced displacive radiation damage. Following the ion implantation, the samples were annealed at 1100 °C for 2 h in either a reducing environment or an oxidizing environment. Some samples were also annealed sequentially in both environments. The reducing environments used included flowing Ar $+4\%H_2$ (ArH_2) in a quartz tube furnace, or UHV (at a pressure of 2×10^{-8} Torr). Flowing O_2 or Ar (99.999% pure) in a quartz furnace were used as oxidizing environments. For anneals carried out in the quartz furnace, the tube was pumped down to a pressure of 4×10^{-6} Torr prior to flowing the desired gas. No attempt was made to further purify the flowing gases or to remove water vapor. The results achieved using flowing Ar were similar to those achieved using flowing O_2. The samples were characterized using 2.3 MeV He^+ Rutherford backscattering (RBS)-channeling measurements and by x-ray diffraction ($Cu\,K_\alpha$ radiation) using a powder diffractometer or a four-circle diffractometer. Selected samples were examined by cross-section transmission electron microscopy (TEM), and the magnetic properties of selected samples were determined using a superconducting quantum interference device (SQUID) magnetometer at a sample temperature of 5 K in applied magnetic fields up to ±65 kOe.

III. RESULTS

Figure 1 compares the x-ray diffraction results obtained from a sample of Fe+Pt implanted Al_2O_3 annealed in a reducing environment [Fig. 1(a)] with those obtained from an identical sample annealed in an oxidizing environment [Fig. 1(b)]. In the as-implanted state (not shown), the only diffraction lines observed from either sample were those expected from the Al_2O_3 substrate. After annealing in the reducing environment ArH_2 [Fig. 1(a)], the θ–2θ scans along the *c*-axis of Al_2O_3 show the expected strong (0006) diffraction line from Al_2O_3. In addition, several other strong lines are seen in the spectra of Fig. 1(a) that correspond to those expected[9] from the chemically ordered, face-centered tetragonal (fct) $L1_0$ phase of FePt. Our previous work[8] established that these FePt nanoparticles have a maximum size of ~25 nm in diameter and that they are oriented with respect to the Al_2O_3 *c*-axis. There are, however, multiple crystallographic orientations for the nanoparticles [i.e., FePt (111), FePt (110), and several other planes parallel to the Al_2O_3 (0001) planes are observed]. In Fig. 1(a), the FePt (110) line is a

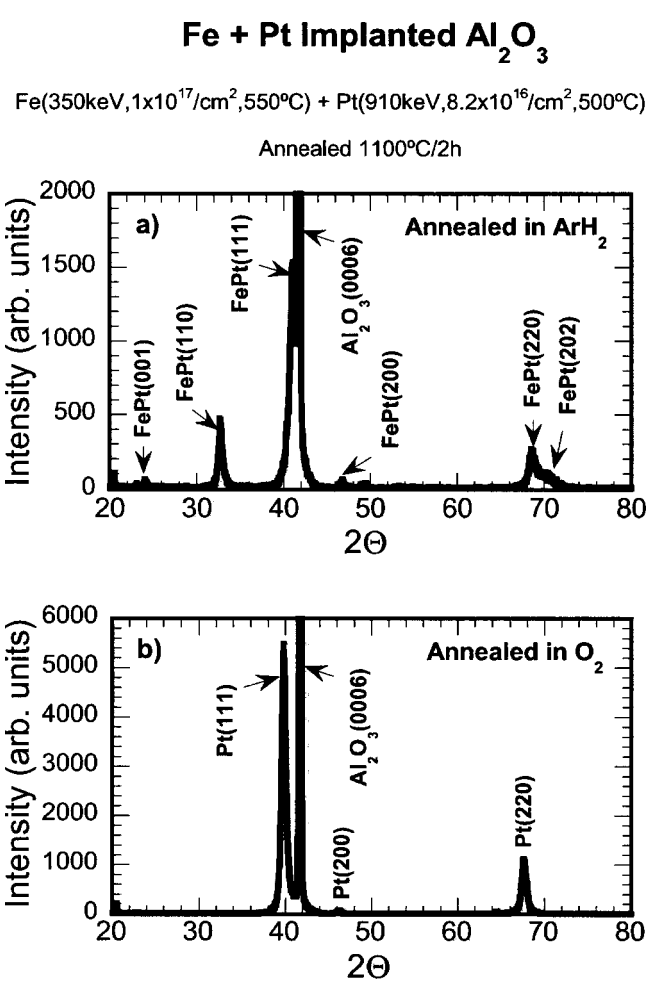

FIG. 1. X-ray diffraction θ–2θ scans along the surface normal for *c*-axis Al_2O_3 crystals implanted by Fe+Pt and annealed at 1100 °C for 2 h in (a) flowing ArH_2 and (b) flowing O_2.

superstructure reflection due to chemical ordering. There is also a weaker superstructure reflection in Fig. 1(a) arising from FePt (001). The presence of these superstructure reflections demonstrates that at least some of the FePt nanoparticles have the ordered $L1_0$ structure expected from fct FePt. The other strong lines identified in Fig. 1(a) are fundamental reflections (allowed even in chemically disordered alloys) from fct FePt. Our previous work[8] also established that the FePt nanoparticles produced by the conditions used in Fig. 1(a) are fully ordered and probably contain some incorporated Al atoms in addition to Fe and Pt.

Annealing an implanted sample in UHV ($\sim2\times10^{-8}$ Torr) also gives rise to the formation of oriented FePt nanoparticles, as demonstrated by x-ray diffraction results (not shown). The same x-ray peaks are observed as those shown in [Fig. 1(a)], and only the relative intensities are different [i.e., there is a greater (111) FePt texture than that shown in Fig. 1(a)]. Therefore, annealing in either flowing ArH_2 or annealing in UHV gives rise to the formation of oriented FePt nanoparticles with the $L1_0$ structure.

Figure 1(b) is a θ–2θ scan from a sample implanted in the same manner as that corresponding to Fig. 1(a) but annealed in an oxidizing environment (flowing O_2). In this case, there are no diffraction lines that can be identified as

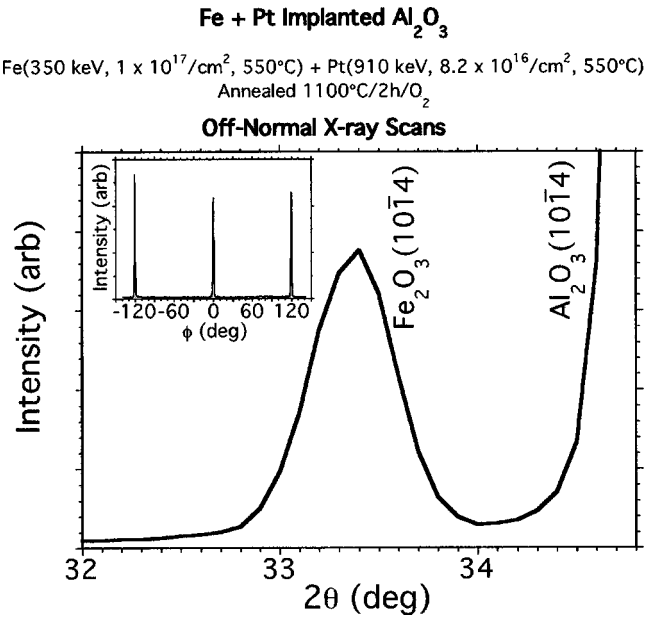

FIG. 2. Off-normal θ–2θ scans through $Al_2O_3\,(10\bar{1}4)$ for *c*-axis Al_2O_3 implanted by Fe+Pt and annealed at 1100 °C for 2 h in flowing O_2. The inset is a ϕ scan through $Fe_2O_3\,(10\bar{1}4)$ reflections demonstrating 120° symmetry.

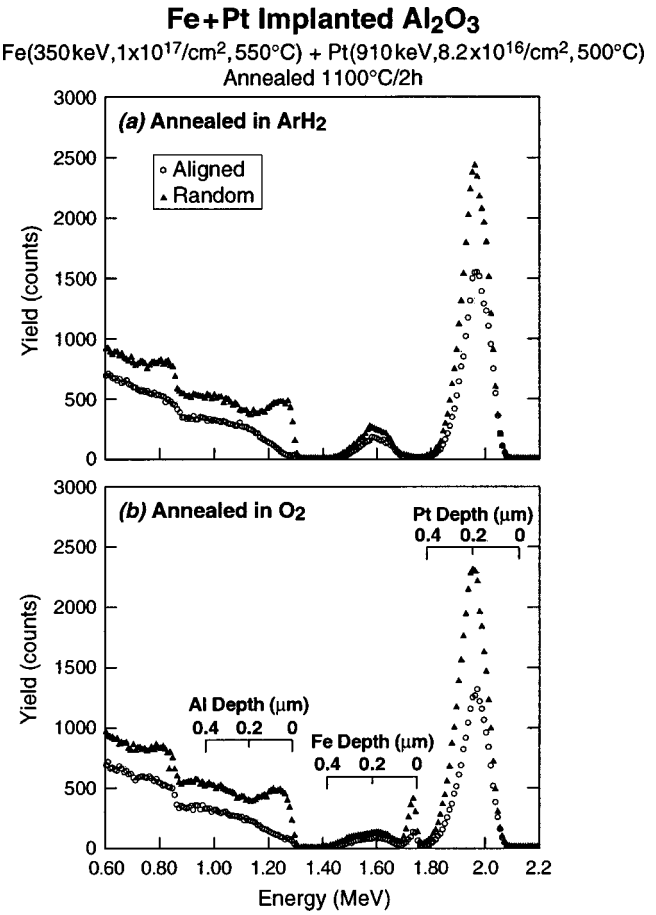

FIG. 3. RBS-chaneling measurements (2.3 MeV He^+ ions) on *c*-axis-oriented Al_2O_3 crystals implanted by Fe+Pt and annealed at 1100 °C for 2 h in (a) flowing ArH_2 and (b) flowing O_2. Depth scales appropriate for Pt, Fe, and Al in Al_2O_3 are indicated.

arising from FePt. In Fig. 1(b), strong Pt (111) and Pt (220) lines and a weak Pt (200) diffraction line are observed in addition to the Al_2O_3 (0006) reflection. This demonstrates that annealing in an oxidizing environment results in the precipitation of Pt to form nanoparticles and that these nanoparticles are oriented with respect to the Al_2O_3 matrix. In Fig. 1(b), the absence of diffraction lines arising from second-phase precipitates containing iron such as α-Fe, Fe_3O_4, FeO, or $FeAl_2O_4$ indicates that very few (if any) oriented nanoparticles of these precipitates are produced (although we cannot rule out the possibility of randomly oriented precipitates). There are several possibilities concerning the implanted Fe. Among these are (a) Fe is lost from the sample by a diffusion process during annealing in the oxidizing environment, (b) Fe forms noncrystalline precipitates, (c) Fe is incorporated into solid solution as a dilute impurity in the Al_2O_3 matrix, and (d) implanted Fe forms some other iron-rich precipitate.

It should be noted that the rhombohedral hematite phase[9] of α-Fe_2O_3 is isostructural with α-Al_2O_3 but has slightly larger lattice parameters than α-Al_2O_3. Consequently, x-ray diffraction peaks from α-Fe_2O_3 occur at slightly lower angles than the corresponding peaks for α-Al_2O_3. If epitaxial precipitates of α-Fe_2O_3 were produced during annealing in flowing O_2, then the most intense peak from Fe_2O_3 in the θ–2θ scan along the surface normal would be expected to be Fe_2O_3 (0006). However, this peak would be nearly coincident with the intense Pt (111) diffraction peak at $2\theta \sim 39.76°$ in Fig. 1(b). Therefore, off-normal x-ray scans using a four-circle diffractometer are required to determine whether epitaxial precipitates of α-Fe_2O_3 are formed. One such scan through $Al_2O_3\,(10\bar{1}4)$ is shown in Fig. 2 for the sample annealed in flowing O_2. In addition to the expected intense peak from Al_2O_3, there is a peak at $2\theta \sim 33.3°$ which we identify as $Fe_2O_3\,(10\bar{1}4)$. The inset in Fig. 2 shows a ϕ scan through the $Fe_2O_3\,(10\bar{1}4)$ reflections. The ϕ scan results exhibit 120° symmetry which implies that the Fe_2O_3 is single domain. Other off-axis x-ray scans were used to identify $Fe_2O_3\,(11\bar{2}6)$, $(02\bar{2}4)$, and $(01\bar{1}8)$ reflections. These results conclusively demonstrate that at least some of the Fe is in the form of α-Fe_2O_3 epitaxial with the α-Al_2O_3 substrate. The α-Fe_2O_3 precipitates have an in-plane mosaic spread of $\Delta\phi \sim 0.7°$ and are, therefore, well-aligned. The correlation length extracted from the full-width half-maximum of a high-resolution x-ray scan through $Fe_2O_3\,(02\bar{2}4)$ is ~33 nm. The off-axis x-ray scans yield rhomohedral Fe_2O_3 lattice parameters of $a = b = 0.502$ nm and $c = 1.364$ nm. Thus, in Fig. 1(b), the expected weak Fe_2O_3 (0006) line is merged with the very intense Pt(111) line.

The results of RBS-channeling measurements made on Fe+Pt implanted Al_2O_3 samples that were annealed in either a reducing or an oxidizing environment are shown in Fig. 3. In the as-implanted state, channeling measurements (not shown) demonstrate that the Al_2O_3 matrix is heavily damaged but not rendered amorphous during elevated-temperature ion implantation. Annealing the samples in ArH_2 [Fig. 3(a)] gives rise to a substantial recovery of the lattice damage, accompanied by significant ion channeling in

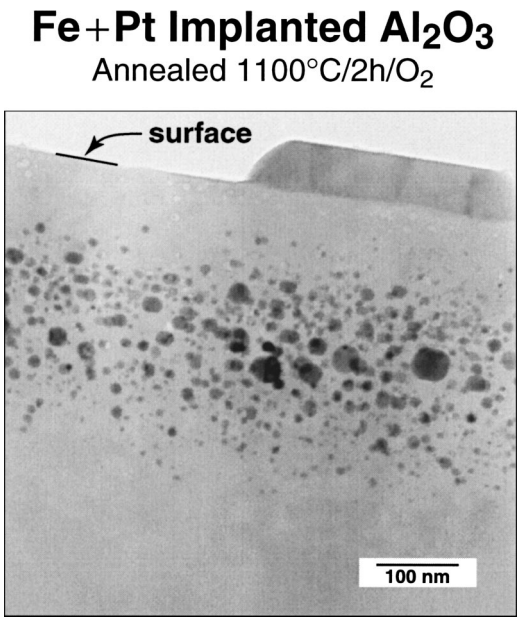

FIG. 4. Cross-section TEM results for *c*-axis-oriented Al_2O_3 implanted by Fe+Pt and annealed in flowing O_2 at 1100 °C for 2 h.

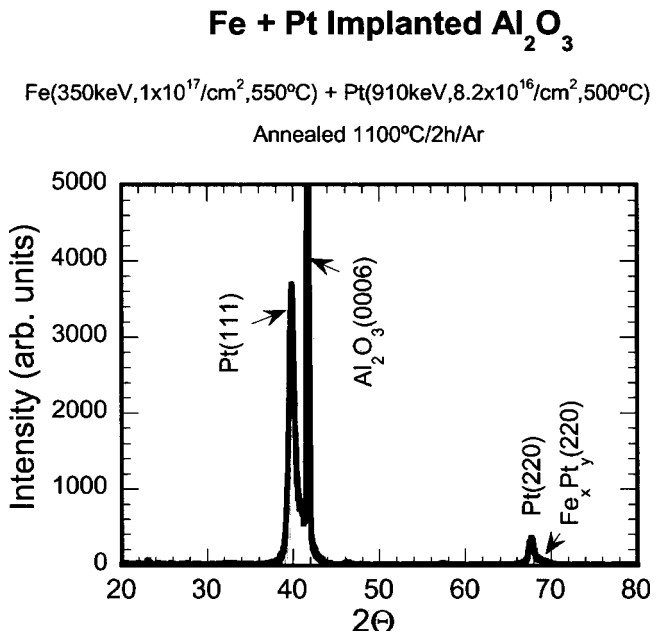

FIG. 5. X-ray diffraction θ–2θ scans along the surface normal for *c*-axis-oriented Al_2O_3 implanted by Fe+Pt and annealed in flowing Ar at 1100 °C for 2 h.

both the Fe and Pt portions of the RBS spectrum. The channeling in the Fe and Pt regions in Fig. 3(a) is due to the formation of oriented FePt nanoparticles during annealing [as also demonstrated by the x-ray results of Fig. 1(a)]. In addition, there is no loss of Fe or Pt, and there is little if any redistribution of the implanted Fe and Pt during annealing in ArH_2.

Annealing in O_2 [Fig. 3(b)] also gives rise to a substantial recovery of the Al_2O_3 lattice damage, and both the Fe and Pt exhibit substantial ion channeling after annealing. The ion channeling in the Pt part of the spectrum is due to the formation of oriented Pt nanoparticles during annealing in O_2 [see Fig. 1(b)]. The RBS results indicate that there is no loss of implanted Fe or Pt during annealing in O_2, and there is little, if any, redistribution of the Pt as a result of annealing. However, ~40% of the implanted Fe is segregated to the surface during annealing in O_2, and this segregated Fe apparently forms the epitaxial Fe_2O_3 precipitates. The ion channeling observed for Fe at the surface is due to channeling in these epitaxial Fe_2O_3 precipitates. The Fe remaining in the bulk also exhibits a channeling effect, consistent with Fe in solid solution (i.e., substitutional) in the matrix.

Figure 4 shows a cross-section TEM micrograph illustrating the microstructure in the near surface of the Fe+Pt implanted Al_2O_3 sample annealed in O_2. The large nanoparticles located at a depth of ~200 nm have a maximum diameter of ~40 nm. Energy dispersive x-ray spectroscopy (EDS) measurements demonstrate these nanoparticles are extremely Pt rich (they may be pure Pt, but extra lines from the matrix could not be completely avoided). These particles are therefore almost certainly the oriented Pt nanoparticles identified by the x-ray diffraction results of Fig. 1(a). The large pancake-shaped ledgelike precipitates on the surface of the sample have a thickness of ~60 nm and extend up to ~300 nm parallel to the surface. RBS and EDS measurements show these to be Fe and O rich and these are believed to be the epitaxial α-Fe_2O_3 precipitates identified by the x-ray results of Fig. 2. Cavities are observed in the region just below the surface, but there are no precipitates present. This region also has a low concentration of Fe (RBS and EDS measurements), and the ion channeling results and equilibrium phase diagrams suggest that this Fe is in solid solution in the matrix.

X-ray diffraction scans along the surface normal for an implanted sample annealed in flowing Ar (99.999%) are shown in Fig. 5. Strong Pt (111) and Pt (220) lines are observed, demonstrating the formation of oriented Pt nanoparticles even when annealing in nominally high purity Ar. There are very weak lines from FePt (220) or $FePt_3$ (220) (identified) as well as a very weak line from FePt (110) (not identified) in the spectrum suggesting that almost all of the nanoparticles formed are Pt with a few Fe_xPt_y alloy nanoparticles. The spectrum shown in Fig. 5 is very similar to that in Fig. 1(b), which was obtained for a sample annealed in flowing O_2. In addition, the RBS-channeling results from this sample are also virtually identical to those obtained from a sample annealed in O_2 [Fig. 3(b)] and almost half the Fe is segregated to the surface. It is likely that the segregated Fe is in the form of epitaxial α-Fe_2O_3 as was found for the sample annealed in O_2 [see Fig. 2]. Thus, the results obtained by annealing in Ar are very similar to those obtained by annealing in O_2. The annealing procedure was carried out in a quartz tube furnace with no additional purification of the Ar gas, so it is likely that oxygen partial pressure from impurities in the gas or from the heated quartz provides enough oxygen for an oxidizing-environment anneal even in flowing high-purity Ar gas.

Different annealing environments and the resulting microstructural changes have a dramatic effect on the ferromagnetic properties of Fe+Pt implanted Al_2O_3 samples. Figure 6

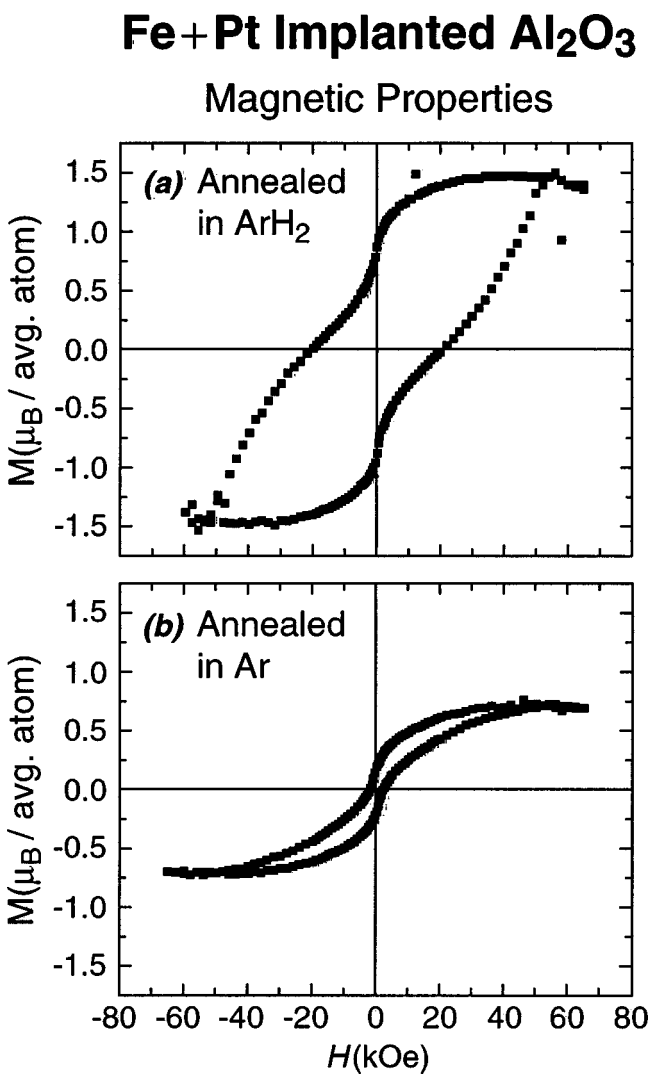

FIG. 6. Magnetization measurements for *c*-axis-oriented Al_2O_3 implanted by Fe+Pt and annealed at 1100 °C for 2 h in (a) flowing ArH_2 and (b) flowing Ar. Measurements were made at $T=5$ K with H applied parallel to the surface normal.

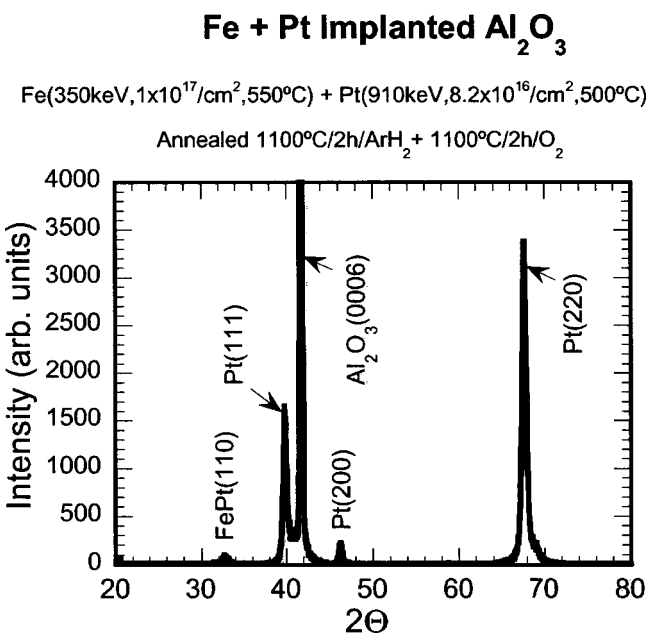

FIG. 7. X-ray diffraction θ–2θ scans along the surface normal for *c*-axis-oriented Al_2O_3 implanted by Fe+Pt and annealed in flowing ArH_2 (1100 °C/2 h) followed by annealing in flowing O_2 (1100 °C/2 h).

shows the magnetization curves measured at $T=5$ K using a SQUID magnetometer for samples annealed in either ArH_2 [Fig. 6(a)] or Ar [Fig. 6(b)]. These curves represent measurements of the magnetic moment of the sample (in units of Bohr magnetons per implanted ion) as the applied field is scanned in the range of +65 to −65 kOe. For these results, the diamagnetic component from the Al_2O_3 substrate has been removed from the data. The hysteresis in the curves of Fig. 6 reflects the presence of ferromagnetic nanoparticles. For the sample annealed in ArH_2, FePt nanoparticles with the $L1_0$ structure are formed, the saturation magnetic moment is very comparable with that in bulk alloys of this composition, and the magnetic coercivity is approximately 23 kOe. For the sample annealed in Ar, the magnetic coercivity is much less (less than 2 kOe), and the saturation magnetization is reduced by a factor of two compared with the results obtained by annealing in ArH_2. For the sample annealed in Ar, Fe is observed in several different forms, which potentially contribute to the observed signal. First, the presence of some disordered Fe_xPt_y alloy nanoparticles can provide a saturating ferromagnetic moment with the low coercivity, less than 2 kOe, seen in Fig. 6(b). An additional contribution comes from isolated Fe^{+3}-ions in solution that, at $T=5$ K, are magnetized reversibly to near-alignment by the large field. [At 300 K, the magnetiztion (not shown) has almost no contribution from the Brillouin-like response of isolated Fe-ions, but the ferromagnetic Fe_xPt_y alloy signal is still present.] Finally, one expects no significant signal from the α-Fe_2O_3 hematite phase, which is antiferromagnetic. While qualitative, this assignment is consistent with the properties of the observed phases in the annealed materials.

FePt nanoparticles with the $L1_0$ structure that are formed in Al_2O_3 by annealing in a reducing environment [Fig. 1(a)] can be decomposed by subsequent annealing in an oxidizing environment. This is shown by the x-ray diffraction results given in Fig. 7. This spectrum was obtained after annealing the sample of Fig. 1(a) for an additional 2 h at 1100 °C in flowing O_2. The first anneal in a reducing environment produced FePt nanoparticles with the ordered $L1_0$ structure. After the subsequent anneal in O_2, the x-ray spectrum was dominated by strong lines arising from Pt with only very weak lines remaining from the original FePt nanoparticles. The Pt lines show that there are multiple orientations of the Pt nanoparticles [i.e., Pt nanoparticles oriented with (111), (220), and (200) planes parallel to the Al_2O_3 *c*-planes are observed]. With the exception of the weak FePt (110) reflection, there are no other lines that can be attributed to Fe-containing compounds in Fig. 7, but it is likely that epitaxial α-Fe_2O_3 precipitates are on the surface since RBS-channeling measurements (not shown) on this sample are nearly identical to the results of Fig. 3(b) showing that the Fe has undergone substantial redistribution with nearly half segregated to the surface (but with no net loss of implanted Fe) during the subsequent annealing in the oxidizing atmosphere.

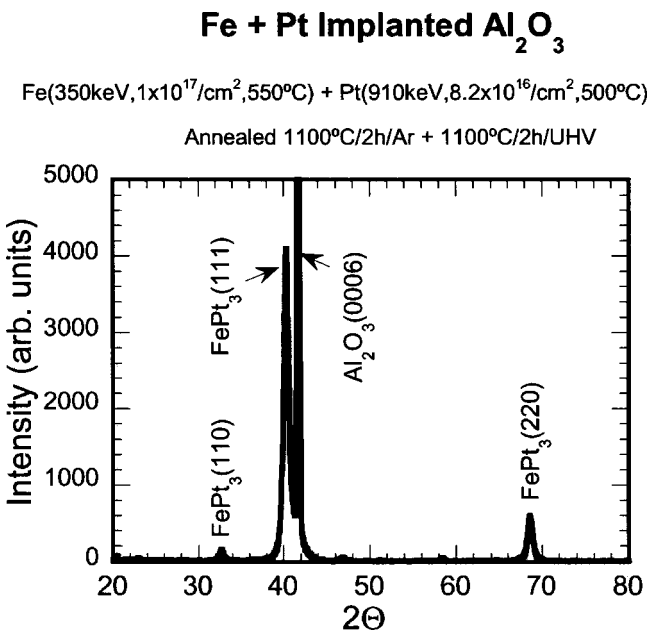

FIG. 8. X-ray diffraction θ–2θ scans along the surface normal for *c*-axis-oriented Al_2O_3 implanted by Fe+Pt and annealed in flowing Ar (1100 °C/2 h) followed by annealing in UHV (2×10^{-8} Torr) for 2 h at 1100 °C.

In addition, the redistributed Fe exhibits a noticeable channeling effect, and some of the redistributed Fe may be incorporated into a solid solution in the Al_2O_3 matrix after the second anneal. Therefore, if Al_2O_3 samples containing ordered FePt nanoparticles are subsequently annealed in an oxidizing environment, the FePt nanoparticles decompose and the results are very similar to those obtained by annealing Fe+Pt-implanted Al_2O_3 in an oxidizing environment.

We have also formed alloy nanoparticles by sequentially annealing Fe+Pt-implanted Al_2O_3 in an oxidizing environment, followed by annealing in a reducing environment as verified by the x-ray diffraction results of Fig. 8. In this case, the implanted crystal was first annealed in an oxidizing environment (flowing Ar) to form oriented Pt nanoparticles with ~40% of the Fe segregated to the surface in the form of epitaxial α-Fe_2O_3 [see Figs. 1(b), 2, and 3]. This sample has ~60% of the Fe remaining in the bulk, most likely in solid solution. When this sample was subsequently annealed in a reducing environment (UHV), the x-ray diffraction results of Fig. 8 show that an ordered alloy was formed, but in this case the alloy formed is the ordered $L1_2$ phase[9] of $FePt_3$, with several orientations of $FePt_3$ nanoparticles relative to the Al_2O_3 host substrate. Formation of the $FePt_3$ nanoparticles occurred with no additional redistribution of Fe (or Pt) as compared to that resulting from the initial annealing in Ar which gave rise to a ~40% segregation of Fe to the surface. The formation of $FePt_3$ instead of FePt alloy nanoparticles in the bulk is reasonable since much of the Fe was segregated to the surface during the initial anneal, and therefore, the local concentration of Fe in the vicinity of the precipitated Pt was considerably less than that required to form nearly equiatomic FePt. Segregated Fe remains on the surface (and is probably in the form of epitaxial precipitates of α-Fe_2O_3) after the subsequent anneal in UHV. From the results presented in Figs. 7 and 8, it appears that one can cycle between forming oriented alloy nanoparticles and the decomposition of the alloy depending on the choice of the final annealing environment. However, segregation of Fe to the surface appears to be irreversible under the conditions studied. This is evidence that equilibrium conditions, and the ''local'' availability of the constituents (Fe+Pt) rather than kinetic effects are responsible for determining the phases formed and the microstructure of the nanocomposite.

IV. DISCUSSION

Results presented in this article demonstrate that oriented $Fe_{55}Pt_{45}$ nanoparticles with the fct $L1_0$ structure are formed in Al_2O_3 by annealing Fe+Pt implanted Al_2O_3 in a reducing environment (flowing ArH_2 or UHV). Nanoparticles formed in this way are ferromagnetic and have a very high magnetic coercivity (in excess of 20 kOe). When similar samples are annealed in an oxidizing environment (such as flowing O_2), oriented Pt nanoparticles are formed. Pt has a very low affinity for oxygen, so it is not surprising that during annealing in an oxidizing environment Pt precipitates are formed in Al_2O_3. Fe will readily combine with oxygen, but it certainly will not reduce Al_2O_3 during the annealing process. However, if excess oxygen is supplied by the annealing environment, then this can combine with the implanted Fe since the affinity of Fe for oxygen is greater than that of Pt.

The implanted Fe redistributes during annealing in an oxidizing environment with ~40% segregating to the surface where it forms epitaxial precipitates of α-Fe_2O_3. The remainder of the Fe remains in the bulk after annealing in O_2 and shows a reasonable ion channeling effect in depth regions where no precipitates are detected by TEM. This is evidence for the formation of a solid solution of the form $(Al_yFe_{1-y})_2O_3$ (with *y* close to unity), in agreement with the predictions[10] of the phase diagram which show that Fe_2O_3 is soluble in Al_2O_3 to concentrations of several percent at 1100 °C.

Several experiments[11–16] have been carried out to investigate the implantation of Fe only into Al_2O_3 (at lower energies and at room temperature or below) followed by annealing in an oxidizing environment. In addition to finding evidence for Fe-containing solid solutions, these studies have revealed a variety of Fe containing precipitates such as α-Fe_2O_3, $FeAl_2O_4$ as well as mixed oxides such as $(Fe_yAl_{1-y})_3O_4$ on the surface or in the interior depending on the dose, energy, implantation temperature, and annealing temperature. A number of these experiments[11,14–16] report that implanted Fe segregates to the surface and forms ledge-like precipitates of α-Fe_2O_3 similar to those that we observe when Al_2O_3 is implanted by Fe+Pt and annealed in an oxidizing environment. Also, when Al_2O_3 is implanted by Fe only and annealed in a reducing environment, experiments have demonstrated that precipitates of α-Fe are formed.[8,11–15,17–20] Precipitates of α-Fe are measured[8,17–20] to be ferromagnetic with a coercivity in the range of 0.1–0.3 kOe (and a saturation moment comparable to that of bulk bcc Fe) if the size exceeds ~7 nm diameter. Below this

size, the α-Fe nanoparticles exhibit superparamagnetic behavior.[14,17,20]

Recently, results have been reported on the films formed by oxygen-plasma-assisted molecular beam epitaxy (MBE) deposition of Fe onto the surface of *c*-axis oriented Al_2O_3.[21] These studies show that oriented films of α-Fe_2O_3, FeO, Fe, or Fe_3O_4 can be deposited on the Al_2O_3 surface depending on growth conditions. If nanoparticles of these species were produced in Al_2O_3 either by Fe implantation alone, or by Fe+Pt implantation, followed by annealing in O_2, then the epitaxial relationships of the oriented nanoparticles should be similar to that of the MBE produced films of Ref. 21. In our experiments on Al_2O_3 implanted by Fe+Pt and annealed in O_2, there is no evidence for second-phase precipitates of any of the species listed above except α-Fe_2O_3.

Our results on sequential annealing of Fe+Pt implanted Al_2O_3 shows that the microstructure and the phase formed is determined by the final annealing environment, and this is evidence of the importance of equilibrium rather than kinetic effects in determining the properties of the nanocomposite. If the initial anneal is in a reducing environment, then oriented FePt nanoparticles with the $L1_0$ structure are produced with little (if any) redistribution of the implanted impurities. Subsequent annealing in an oxidizing environment decomposes the FePt nanoparticles and results in Pt precipitation accompanied by Fe redistribution with significant segregation of Fe to the surface. If the initial anneal is in an oxidizing environment, this gives rise to the precipitation of Pt nanoparticles accompanied by segregation of ~40% of the Fe to the surface where it forms epitaxial α-Fe_2O_3 precipitates with the remainder of the Fe remaining in solution in the bulk. Subsequent annealing in a reducing environment gives rise to the formation of an ordered alloy ($FePt_3$) in the bulk with the segregated Fe remaining on the surface. In this case, the alloy formed is $FePt_3$ rather than FePt because the local concentration of Fe in the vicinity of the Pt precipitates was considerably reduced by segregation in the initial anneal. The subsequent anneal in a reducing environment then led to the interaction of the Pt with the Fe in solution. (In previous work,[8] we demonstrated that $FePt_3$ nanoparticles could be formed by the implantation of Fe and Pt in a ratio of 1:3, followed by annealing in ArH_2). However, it is somewhat surprising that Pt can remove Fe from solid solution in Al_2O_3 during annealing in ArH_2 and further work is required to clarify this behavior.

V. CONCLUSIONS

We have shown that the structural and magnetic properties of near-surface FePt nanocomposites in Al_2O_3 can be controlled by variations of the annealing conditions following the implantation of Fe and Pt. In particular, $L1_0$ FePt nanoparticles with the very high magnetic coercivity that is desirable for applications can be formed in Al_2O_3 by the ion implantation of Fe+Pt in overlapping profiles, followed by annealing in a reducing environment. It is essential to anneal in a reducing environment in order to form the ordered alloy and to produce nanoparticles with high magnetic coercivity. FePt ordered alloy nanoparticles with the $L1_0$ structure will not form during annealing in an oxidizing environment. The strong dependence of properties on the annealing environment is not limited to the case of Fe+Pt alone. We have also investigated[22] nanoparticle formation for the case of Co+Pt implantation of Al_2O_3. We find that annealing in a reducing environment is essential for forming ferromagnetic ordered alloy nanoarticles for CoPt in Al_2O_3 also. Details of the effect of the annealing environment on CoPt nanoparticle formation will be reported separately.

ACKNOWLEDGMENT

Oak Ridge National Laboratory is managed by UT-Battelle, LLC, for the U.S. Dept. of Energy under Contract No. DE-AC05-00OR22725.

[1] S. Sun, C. B. Murray, D. Weller, L. Folks, and A. Moser, Science **287**, 1989 (2000); see also S. Sun, E. E. Fullerton, D. Weller, and C. B. Murray, IEEE Trans. Magn. **37**, 1239 (2001).
[2] D. Weller, A. Moser, L. Folks, M. E. Best, W. Lee, M. F. Toney, M. Schwickert, J.-U. Thiele, and M. F. Doerner, IEEE Trans. Magn. **36**, 10 (2000).
[3] R. F. C. Farrow, D. Weller, R. F. Marks, M. F. Toney, D. J. Smith, and M. R. McCartney, J. Appl. Phys. **84**, 934 (1998).
[4] M. R. Visokay and R. Sinclair, Appl. Phys. Lett. **66**, 1692 (1995).
[5] B. M. Lairson, M. R. Visokay, R. Sinclair, and B. M. Clemens, Appl. Phys. Lett. **62**, 639 (1993).
[6] D. Ravelosona, C. Chappert, V. Mathet, and H. Bernas, Appl. Phys. Lett. **76**, 236 (2000).
[7] C. W. White, S. P. Withrow, J. D. Budai, L. A. Boatner, K. D. Sorge, J. R. Thompson, K. S. Beaty, and A. Meldrum, Nucl. Instrum. Methods Phys. Res. B **191**, 437 (2002).
[8] C. W. White, S. P. Withrow, K. D. Sorge, A. Meldrum, J. D. Budai, J. R. Thompson, and L. A. Boatner, J. Appl. Phys. **93**, 5656 (2003).
[9] *JCPDS—International Center for Diffraction Data, Powder Diffraction Files #43-1359, #04-0802, #86-2368, #29-0716* (ICDD, Newton Square, PA, 2000).
[10] E. R. Levin, C. R. Robbins, and H. F. McMurdie, *Phase Diagrams for Ceramists* (American Ceramic Society, Columbuo, OH, 1979), p. 43.
[11] C. J. McHargue, G. C. Farlow, P. S. Sklad, and C. W. White, Nucl. Instrum. Methods Phys. Res. B **19/20**, 813 (1987).
[12] J. C. McCallum, C. W. White, P. S. Sklad, and C. J. McHargue, Nucl. Instrum. Methods Phys. Res. B **46**, 137 (1990).
[13] G. C. Farlow, P. S. Sklad, C. W. White, and C. J. McHargue, J. Mater. Res. **5**, 1502 (1990).
[14] C. J. McHargue, P. S. Sklad, C. W. White, G. C. Farlow, A. Perez, and G. Marest, J. Mater. Res. **6**, 2145 (1991).
[15] P. S. Sklad, C. J. McHargue, C. W. White, and G. C. Farlow, J. Mater. Sci. **27**, 5895 (1992).
[16] T. Kobayashi and T. Terai, Nucl. Instrum. Methods Phys. Res. B **148**, 159 (1999).
[17] M. Ohkubo, T. Hioki, and J. Kawamoto, J. Appl. Phys. **62**, 3069 (1987).
[18] H.-G. Jang, H.-B. Kim, J.-H. Joo, C.-N. Whang, H.-K. Kim, D.-W. Moon, J. J. Woo, and S.-O. Kim, Nucl. Instrum. Methods Phys. Res. B **124**, 528 (1997).
[19] E. Alves, C. J. McHargue, R. C. Silva, C. Jesus, O. Conde, M. F. da Silva, and J. C. Soares, Surf. Coat. Technol. **128–129**, 434 (2000).
[20] M. Ohkubo, T. Hioki, N. Suzuki, T. Ishiguro, and J. Kawamoto, Nucl. Instrum. Methods Phys. Res. B **39**, 675 (1989).
[21] R. F. C. Farrow, P. M. Rice, M. F. Toney, R. F. Marks, J. A. Hedstrom, R. Stephenson, M. J. Carey, and A. J. Kellock, J. Appl. Phys. **93**, 5626 (2003).
[22] S. P. Withrow, C. W. White, J. D. Budai, L. A. Boatner, K. D. Sorge, J. R. Thompson, and R. Kalyanaraman, J. Magn. Magn. Mater. **260**, 319 (2003).